Proceedings of OMAE2005
24th International Conference on Offshore Mechanics and Arctic Engineering (OMAE 2005)
June 12-17, 2005, Halkidiki, Greece

OMAE2005-67263

CFD analysis of vortex-induced motions of bare and straked cylinders in currents

K P Thiagarajan[1*], Y Constantinides[2] and L Finn[3],
[1]School of Oil & Gas Engineering.The University of Western Australia, Crawley, WA 6009, AUSTRALIA
[2]Chevron Texaco, 2811 Hayes Road, Houston TX 77082, USA
[3]Technip Offshore, Inc. 11700 Old Katy Road, Houston, TX 77079, USA

ABSTRACT

It is widely acknowledged that the use of helical strakes for mitigation of vortex-induced motions (VIM) of surface piercing cylinders, such as spar platforms, is only partially effective. Using computational fluid dynamics tools, we compare the oscillation characteristics of a bare cylinder and a straked cylinder in uniform currents.

Our model comprised of a straked cylinder with diameter of 0.741 m, aspect ratio of 1:1.9 and three helical strakes of height 13% of cylinder diameter. This geometry corresponds to the hard tank geometry of a scaled truss spar model known to exhibit VIM in tow tank testing. In the CFD simulations the cylinder is moored with linear springs to provide a range of reduced velocities. The fluid domain is made of an unstructured grid comprising of hexahedral elements. Fluid structure interaction utilizes grid stretching and a user defined function for solving the equations of motion. Turbulence modeling uses Detached Eddy Simulation (DES) and the boundary layer is modeled using a wall function with a surface roughness of 0.0003 m. Reynolds numbers are in the range of 50,000 to 100,000.

Results for straked cylinder compares reasonably with published results, but under-predicts the peak response. In comparing with corresponding results for a bare cylinder without strakes, the spectral features of the transverse displacement show variations, which are found to be due to the spoiling effect of the strakes.

INTRODUCTION

It is well known in the offshore community that cylindrical bluff structures such as spar platforms suffer from vortex-induced motions (VIM) in strong current conditions. Specifically, the loop current condition in the Gulf of Mexico, where current speeds may exceed 4 knots (2.05 m/s), can create a conducive environment for VIM in spars. All the classic spars in the Gulf of Mexico have recorded VIM in strong loop conditions (Yung et al. 2004). Helical strakes have been used on spars to reduce these motions. These strakes are normally three-stranded, extending over the lower two-thirds of the spar hull. The height is typically 10% of the spar diameter (Yung et al. 2004).

The effectiveness of strakes on spars has not been as remarkable as in air, leading one to contemplate if the basic physics of the problem may have been overlooked. The strakes around a cylinder work by disrupting the correlation of vortices along the length, thus reducing the net transverse force on the cylinder induced by the flow. Bearman and Brankovic (2004) argue that the strakes may work by way of introducing three-dimensionality in the separated flow and destroying regularity of vortex shedding. Experience with risers and spar platforms indicates that strakes suppress the motion to some extent, at the penalty of considerable increase in drag forces on the structure. The latter can have implications on the mooring loads for a spar platform. Irani and Finn (2005) have conducted model tests on a truss spar platform with different strake configurations. They conclude that the geometry and orientation of strakes can be optimized for maximum performance.

Bearman and Brankovic (2004) conducted experiments on cylinders with passive controllers of vortex-induced vibration (VIV). Their cylinder models were of diameter 0.044 m, and length 0.6 m giving an aspect ratio of 1:13.6. The experiments covered a mass ratio of 2.58 and Reynolds numbers in the range 10^3 – 10^4. They found that strakes were more effective than bumps on cylinders in reducing the magnitude of vibration.

* Corresponding author, krish.thiagarajan@uwa.edu.au

However, their conclusion was that the performance of strakes in water was not as effective as in air. Their reasoning based on simple theoretical development of Bearman (1984) is explored further in the present paper.

Moored structures in the ocean such as truss spars exhibit motions in all six degrees of freedom. However, it is principally the horizontal plane translations (surge and sway) that are influenced by VIM. Jauvtis and Williamson (2004) studied the VIV motions of a smooth cylinder with two degrees of freedom at low Reynolds numbers. Their experimental program involved studying cylinders of diameters ranging from 38 – 50 mm and aspect ratios varying from 1:7 – 1:10. Results showed negligible influence of inline motions on the transverse motions for cylinders with high mass ratios greater than 6. For lower mass ratio cylinders, there was a remarkable increase in transverse VIV amplitudes of up to 1.5 diameters. Accompanying this was a modified flow field around the cylinder made up of three vortices for ever half cycle, which the authors labeled as the "2T" mode of vortex shedding.

We study the vortex-induced motions of bare cylinders and straked cylinders using computational fluid dynamics (CFD) tools. The cylindrical structures used here resemble the hard tank of a truss spar model described by Irani and Finn (2005). A companion paper by Halkyard et al. (2005) provides the benchmark study of CFD with model experiments, as well as examines the influence of current direction on the VIM of straked cylinders.

THEORETICAL DEVELOPMENT

Sumer and Fredsoe (1997) show through dimensional analysis that the governing non-dimensional parameters for VIV of a long flexibly mounted cylinder of diameter D in a current of velocity U are:

V_{rn}, M, Ks, Re and k_s/D

For three dimensional cylinders such as spars, one logical extension will be to add the aspect ratio (D/h; h – cylinder draft) as an additional parameter. Here, the mass ratio M is defined as the ratio of the total mass of the cylinder to the displaced mass.

$$M = \frac{m + m_a}{\rho \pi D^2 h / 4} \tag{1}$$

m_a is the still water added mass, taken to be equal to the cylinder displacement. The stability parameter Ks is defined as

$$Ks = 4\pi M \zeta_s \tag{2}$$

where ζ_s is the damping ratio defined in the usual way as the system damping to critical damping ratio. The nominal reduced velocity (V_{rn}) is defined in terms of the natural frequency f_n of the cylinder.

$$V_{rn} = \frac{U}{f_n D} \tag{3}$$

Here f_n is the oscillating natural frequency in water using an added mass coefficient of 1. We contrast the reduced velocity in Eq. (3) with the alternate that is defined in terms of the oscillation frequency f_v.

$$V_r = \frac{1}{St} = \frac{U}{f_v D} \tag{4}$$

where St is the Strouhal number. The remaining parameters are the Reynolds number Re, and the roughness k_s on the cylinder.

The governing equation for one-degree of freedom motion of a cylinder subject to a force may be written as (Sumer and Fredsoe, 1997; Sec. 8.3.2):

$$(m + m_a)\ddot{y}(t) + c\dot{y}(t) + ky(t) = F_l(t) \tag{5}$$

where c is the damping coefficient and k is the stiffness. The lift force on the right hand side of the equation excludes the inertial forces that are implicit in the added mass term m_a. Following the methodology of Bearman (1984), the above equation may be rewritten in terms of the natural frequency f_n, the damping ratio ζ_s and the lift coefficient $C_l(t)$ as follows:

$$\ddot{y}(t) + 4\pi f_n \zeta_s \dot{y}(t) + 4\pi^2 f_n^2 y(t) = C_l(t) \frac{\rho D h U^2}{2(m + m_a)} \tag{6}$$

where the main difference with Bearman's (1984) formulation is the explicit introduction of the added mass here. If the lift force leads the displacement by an angle ϕ, then we may write

$$\begin{aligned} y(t) &= A \sin(2\pi f_v t) \\ C_l(t) &= \bar{C}_l \sin(2\pi f_v t + \phi) \end{aligned} \tag{7}$$

where f_v is the frequency of the vortex-induced motion. Substitution into the equation of motion results in the following equations

$$\frac{f_n}{f_v} = \left[1 - \frac{\bar{C}_l}{2\pi^3} \cos\phi \frac{V_{rn}^2}{M\,(A/D)} \right]^{-1/2} \tag{8}$$

$$\frac{A}{D} = \frac{\bar{C}_l}{\pi^2} \sin\phi \frac{V_{rn}^2}{Ks} \frac{f_n}{f_v} \tag{9}$$

The strakes perform as spoilers by upsetting the spanwise correlation of the phase angle ϕ, and/or reduce the lift coefficient. Bearman and Brankovic (2004) argue that the reason why strakes are not effective in water is because of the low value of the mass parameter M and the stability parameter for neutrally buoyant, lightly damped systems, which makes the denominator of Eq. (9) small.

SPAR GEOMETRY

The two models considered here comprise of a cylindrical structure with and without strakes. The diameter and length of both models are the same and given in Table 1. For the model with strakes, three strakes on the hard tank spiraling counter clockwise at 120 deg around the hard tank over the height

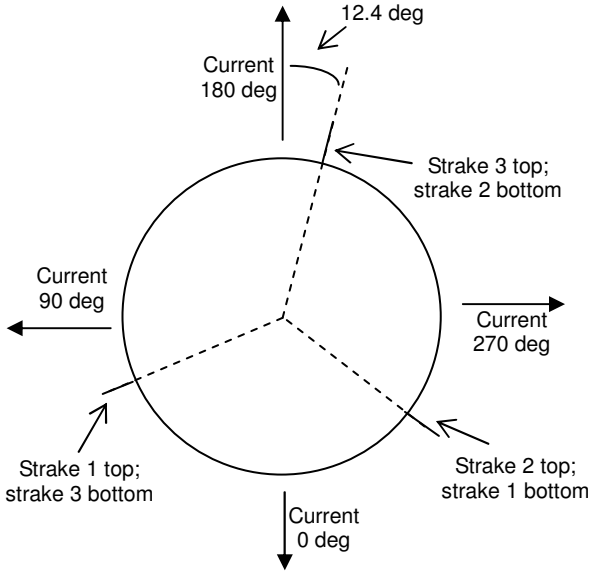

Figure 1. Definition of strake orientation and current direction

specified in Table 1 are considered. The arrangement is shown in Figure 2. Since the cylinder was modelled in CFD without the truss structure, the mass was correspondingly increased to 897 kg. Assuming a theoretical value for the added mass = 598 kg, we get a mass ratio of 2.5. The restoring stiffnesses in the *x* and *y* directions were varied to give rise to various reduced velocity (V_{rn}) values from 4 – 12 (Table 2). The current velocity was fixed at 0.18 m/s for the straked cylinder and 0.21 m/s for the bare cylinder. The direction of current for the straked cylinder was fixed at 157.5 deg which was found from experiments to create high VIM response. All models in the computation had a roughness height of 0.0003 m.

COMPUTATIONAL PROGRAM AND SETUP

The incompressible flow solver AcuSolve™ was used for the computations presented herein. AcuSolve™ is a finite element solver based on the Galerkin/Least Squares formulation. It is second order accurate in time and space and utilizes a fully coupled pressure/velocity iterative solver.

The incompressible Navier-Stokes equations that express the conservation of mass and momentum are shown below:

$$\nabla \cdot u = 0 \tag{10}$$

$$\frac{Du}{Dt} = -\frac{1}{\rho_0}\nabla P' + \nu \nabla^2 u \,. \tag{11}$$

Turbulence was modeled using Spalart's Detached Eddy Simulation (DES) model. DES is based on a hybrid Unsteady Reynolds average Navier-Stokes (URANS) and Large Eddy Simulation (LES) formulation. The URANS turbulence model is based on the one equation turbulence model of Spalart-

Table 1. Spar geometric details

Cylinder diameter (D)	0.741 m	2.431 ft
Cylinder length	1.387 m	4.55 ft
Center well	0.32 m x 0.32 m	1.05ft x 1.05ft
Strake height (13%D)	0.097 m	0.317 ft
Strake starting depth (from free surface)	0.268 m	0.88 ft
Strake ending depth (from free surface)	1.387 m	4.55 ft
Strake starting point (clockwise from the 180 deg current direction)	12.4 deg	
No. of strakes	3	
Strake pitch	3.36 m	11.025 ft

.

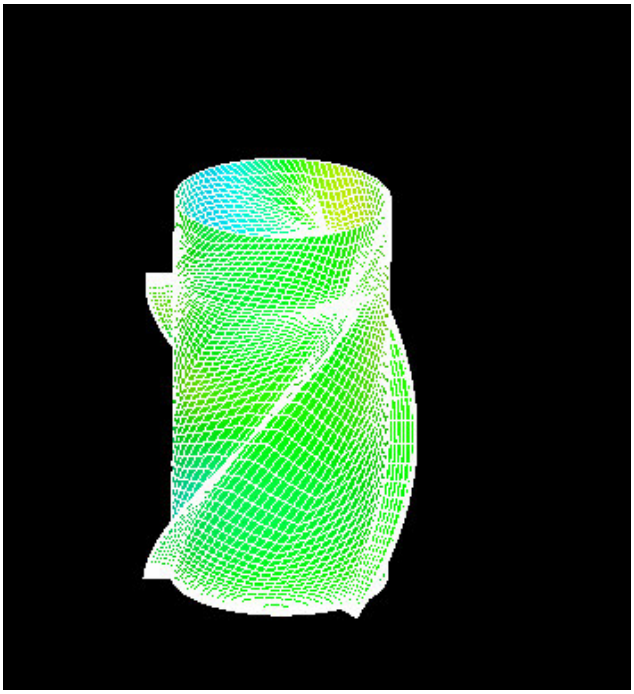

Figure 2. Hard tank surface plot showing high (yellow) and low (blue) pressure regions.

Allmaras (1992). The change in eddy viscosity in the DES model is governed by:

$$\frac{D\tilde{\nu}}{Dt} = C_{b1}\tilde{S}\tilde{\nu} + \frac{1}{\sigma}(\nabla \cdot ((\nu + \tilde{\nu})\nabla\tilde{\nu}) + C_{b2}(\nabla\tilde{\nu})^2) - C_{w1}f_w\left(\frac{\tilde{\nu}}{d}\right)^2 \tag{12}$$

Where $\tilde{\nu}$ is a working variable used to obtain the eddy viscosity and

$$\nu_t = \tilde{\nu} f_{v1} \;; \quad f_{v1} = \frac{\chi^3}{\chi^3 + C_{v1}^3} \;; \quad \chi = \frac{\tilde{\nu}}{\nu} \tag{13}$$

The DES turbulence model is obtained by replacing the distance to the wall d with the minimum of the distance to the wall and a measure of the element size ($C_{des}\Delta$). Near the wall the model acts like the S-A URANS model and far from the wall it behaves similar to LES. The transition between URANS and LES is smooth. A more detailed description of the model can be found in Spalart and Allmaras (1992) as well as the values of the constants in the equations above.

The mesh constructed to capture the flow around the cylinder consisted of about 500,000 hexahedral elements. The mesh included the cylinder with a free surface on the top. Since waves are not important for this case, the free surface was simulated with a fixed boundary having a free slip boundary condition. This prohibits the generation of waves but captures the free flow at the top. The mesh was economized having the majority of elements located in the areas of interest, near the cylinder and in the near wake. The wall roughness was modeled using wall roughness. Wall functions reduce the model size by providing a model for the flow between the wall and logarithmic area of the boundary layer. Typically the first element was placed between y^+ of 30 to 100, that is consistent with most URANS guidelines

The free body motion of the cylinder within the mesh was accommodated using a specified mesh motion in which the position of each node is specified based on the spar position. This approach avoids the solution of nodal locations using an arbitrary elastic solid to represent the mesh (Arbitrary Langrangian Eulerian or ALE method) and hence solve for the new nodal locations. However, the fluid flow is calculated based on the new nodal locations as in the ALE method.

All simulations were performed on ChevronTexaco's Linux cluster using 14 Intel Xeon processors, clocked at 3.06 GHz. Typical runs required about 24 hours of computer time for about 30 oscillation cycles.

RESULTS AND DISCUSSION

We first compare the time series and spectral data for the bare cylinder and the straked cylinder. The cases shown are for V_{rn} = 7 and 6 respectively for the bare and straked cylinders. The time series of the bare cylinder (Figure 3) is approximately sinusoidal with spectral peak at 28 sec, reasonably close to the theoretical natural period of the cylinder. We note that because of the limited length of the time series, the FFT data is sparsely populated in the long period range, and hence the true peak may be in the vicinity of the peak shown in the figures. On the other hand, the straked cylinder shows a modulated signal, and the spectrum in Figure 6 shows two dominant peaks, neither of whose amplitude corresponds to A_{max}/D in Figure 5. In fact, it is the constructive interference of these two frequency components that give rise to the maximum A/D.

Table 2. Computational run parameters

Configuration	V m/s	Kx N/m	Ky N/m	fn Hz	Tn s	Vrn
Bare cylinder	0.21	216.4	201.8	0.06	17.1	4.8
	0.21	96.2	89.7	0.04	25.7	7.3
	0.21	70.7	65.9	0.03	29.9	8.5
	0.21	54.1	50.5	0.03	34.2	9.7
	0.21	34.6	32.3	0.02	42.8	12.1
straked	0.18	216.4	201.8	0.06	17.1	4.2
	0.18	138.5	129.2	0.05	21.4	5.2
	0.18	96.2	89.7	0.04	25.7	6.2
	0.18	70.7	65.9	0.03	29.9	7.3
	0.18	54.1	50.5	0.03	34.2	8.3
	0.18	34.6	32.3	0.02	42.8	10.4
	0.18	24.0	22.4	0.02	51.3	12.5

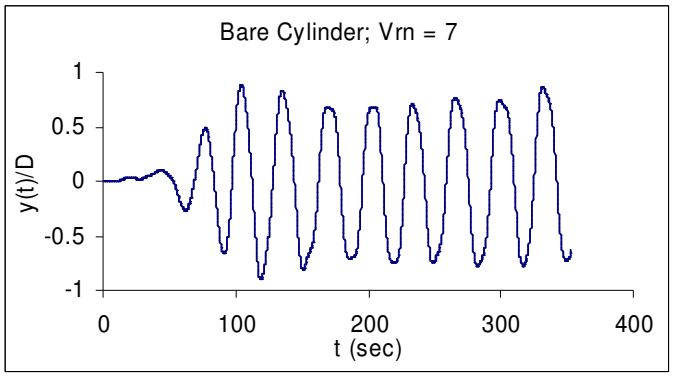

Figure 3. Bare cylinder at V_{rn} = 7, time series plot of transverse displacement

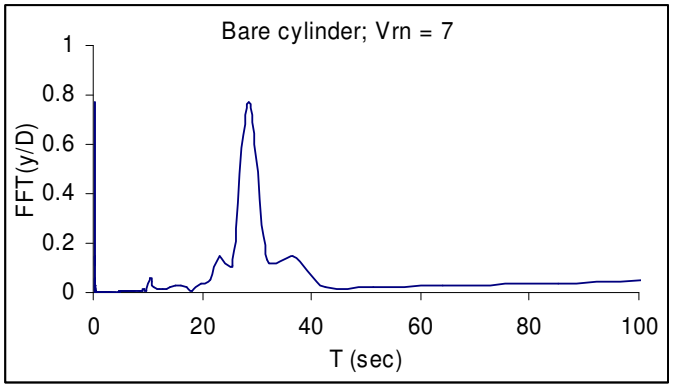

Figure 4. Bare cylinder at V_{rn} = 7, spectral plot of transverse displacement

It is interesting to examine the periods at which these two peaks occur. We hypothesize the second peak at 32 s in Figure 6 to be close to the natural period of the cylinder, giving some allowance due to the paucity of data in the long period range. Further, the second peak appears to correspond closely with the

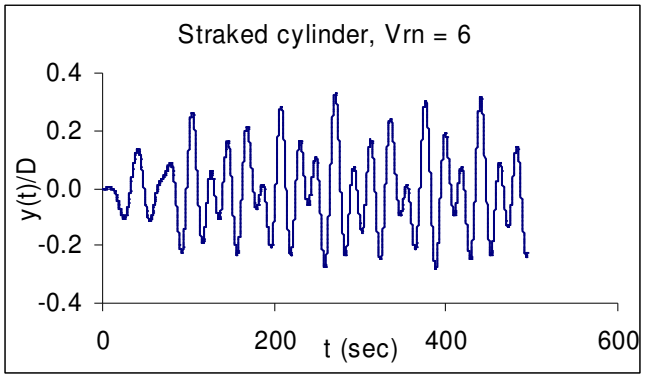

Figure 5. Straked cylinder at V_{rn} = 6, time series plot of transverse displacement

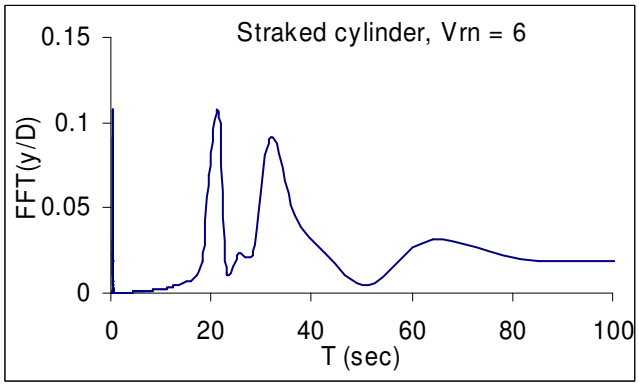

Figure 6. Straked cylinder at V_{rn} = 6, spectral plot of transverse displacement.

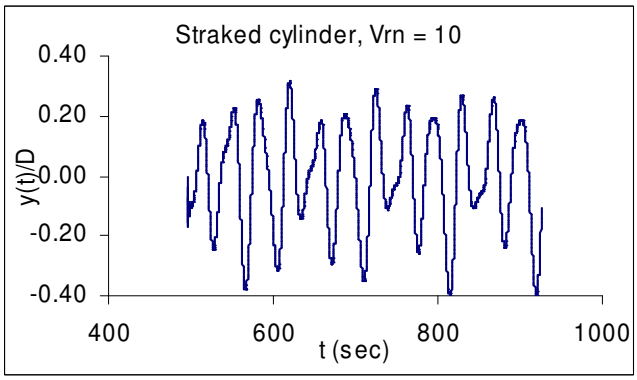

Figure 7. Straked cylinder at V_{rn} = 10, time series plot of transverse displacement

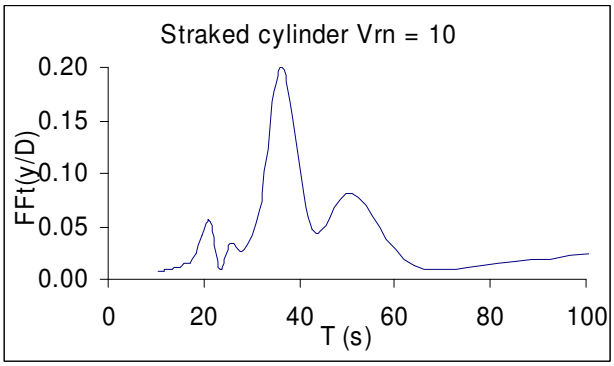

Figure 8. Straked cylinder at V_{rn} = 6, spectral plot of transverse displacement.

peak of the bare cylinder and has a similar broad shape. The first peak is much narrower, and occurs at 21 s, which corresponds to a reduced velocity of 5.1. In other words this period correlates well with the vortex shedding frequency corresponding to a Strouhal number of 0.2. To verify this further, Figures 7 and 8 show the time series and spectral plots for the straked cylinder at V_{rn} = 10. As noted earlier, the change in V_{rn} is effected by reducing the stiffness while keeping the current speed a constant. It is apparent from Figure 8 that the first peak, although smaller, remains at 21 s, while the second peak corresponding to the natural period has shifted further towards 37 s. It is thus becoming apparent that partial lock-in may occur because of the presence of the helical strakes. When lock-in is diminished, the cylinder oscillates at the vortex shedding frequency. As the amplitude picks up and the cylinder locks in it oscillates at the natural period. But then the strakes spoil the flow, resulting in the cylinder reverting to oscillating at the vortex shedding frequency. The flow here appears bifurcated. The modulation of the signal results in the third peak at around 60 sec in Figure 6, which can be seen to be the difference frequency effect of the two peaks.

Figure 9 shows the maximum transverse amplitude for the smooth and straked cylinder and compares with results from experiments of Jauvtis and Williamson (2004) and Bearman and Brankovic (2004). There are considerable differences in the data for the bare cylinder, which would be expected, since the experiments were conducted on smooth cylinders at Reynolds numbers less than 15,000. The data of Williamson shows the curve at the upper branch, which seems to be followed by our CFD results but at much higher values of reduced velocity. The results of Bearman show a transition to the lower branch, presumably because of different mass ratio and damping parameters. Interestingly, the agreement with straked cylinders is reasonable except at the peak value in Figure 10. Our CFD results show a maximum A/D of under 0.4 while experiments are higher, up to 0.55 at a V_{rn} of 5. It should be noted that the experimental model was a long cylinder unlike a spar, and had strakes covering the top third of the length. In contrast the CFD model had strakes covering the lower two-thirds, and had a much smaller aspect ratio. These could be the contributing factors for the differences in Figure 10.

CONCLUSIONS

It is widely acknowledged that computational fluid mechanics tools are enabling technologies for solving offshore industry problems such as vortex-induced motions. VIM on

spars in particular have gained recent attention, and efforts towards predicting the problem satisfactorily are ongoing at various organizations. The present paper has presented one such CFD tool Acusim to solving the VIM problem.

We compared in this paper the displacement of bare cylinders and those equipped with helical strakes as spoilers. The main difference in the spectral data of the transverse displacement between the two configurations is the presence of an additional peak in the latter configuration, corresponding to the Strouhal frequency. The hypothesis then is that due to the partial effectiveness of the strakes (arising from the low mass ratio and stability parameter) the flow appears to switch from a low lock-in to a high lock-in, wherein the frequency of oscillation shifts from the Strouhal frequency to the natural frequency. This also results in modulation of the displacement signal.

Comparison of A/D ratio vs. reduced velocity with published data shows moderate agreement for the bare cylinder, and comparatively better agreement for the straked cylinder.

Research is ongoing to visualize the flow around the cylinders using CFD, in particular to identify the 2T mode discussed by Jauvtis and Williamson (2004). Further, CFD tools will be used to visualize the flow around the strakes and identify the transition between the two frequencies of oscillation. These will be presented in future publications.

ACKNOWLEDGEMENTS

The first author gratefully acknowledges the funding support of Technip Offshore, Inc. Houston. The computational resources for the simulations were provided by the Linux cluster resident in Chevron Texaco Offices in Houston.

REFERENCES

Bearman, P. W., (1984) "Vortex shedding from oscillating bluff bodies", *Ann Rev. Fluid Mech.*, vol. 16, pp 195 – 222.

Bearman, P. W. and Brankovic, M., (2004), "Passive control of vortex-induced vibration," *Eur. J. Mech. B/ Fluids*, vol. 23, Iss. 1, pp 9 – 15.

Halkyard, J., Sirnivas, S., Holmes, S., Constantinides, Y., Oakley, O., and Thiagarajan, K., (2005) "Benchmarking of truss spar vortex-induced motions derived from CFD with experiments," *Proceedings* 24th OMAE, Paper 67252, Halkidiki, Greece.

Irani, M. and Finn, L. (2005) "Improved strake design for vortex-induced motions of spar platforms," *Proceedings* 24th OMAE, Paper 67384, Halkidiki, Greece.

Jauvtis, N. and Williamson, C. H. K., (2004) "The effect of two degrees of freedom on vortex-induced vibration at low mass and damping," *J. Fluid Mech.*, vol. 509, pp. 23 – 62.

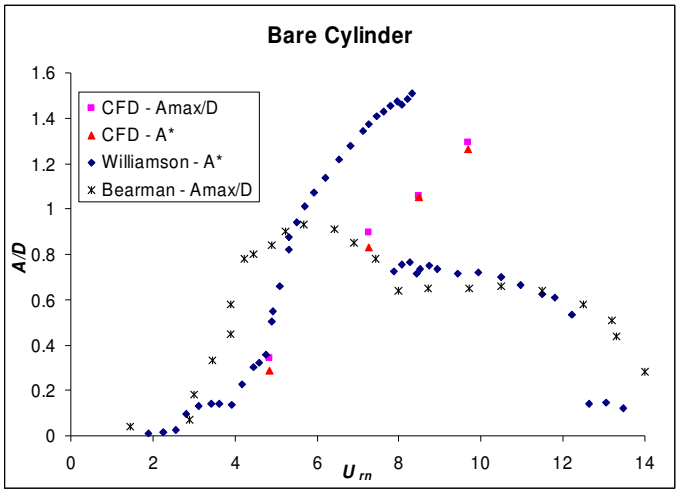

Figure 9. Bare Cylinder A/D vs reduced velocity.

Note: $A^* = \sqrt{2}\frac{A_{max}}{D}$

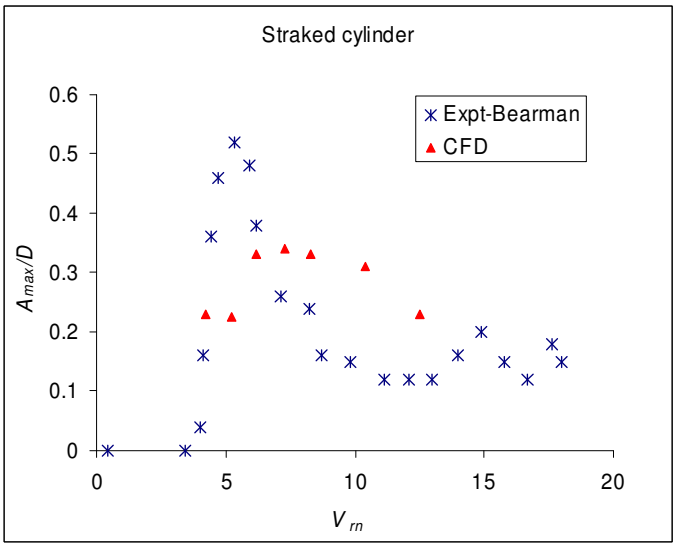

Figure 10. Straked cylinder Amax/D vs. reduced velocity.

Spalart, P.R., and Allmaras, S.R., (1992) "A One-Equation Turbulence Model for Aerodynamics Flows", *AIAA Jl*, Paper 92-0439.

Sumer, B. M. & Fredsoe, J. (1997), *Hydrodynamics Around Cylindrical Structures*, World Scientific Publishing, London.

Yung, T. W., Sandstrom, R. E., Slocum, S. T., Ding, Z. J. and Lokken, R. T., (2004) "Advancement in spar VIV prediction", *Proceedings* Offshore Tech Conf. Paper no. 16343.